Agricultural and Forest Meteorology 314 (2022) 108780

Contents lists available at ScienceDirect

Agricultural and Forest Meteorology

journal homepage: www.elsevier.com/locate/agrformet

Greenup dates change across a temperate forest-grassland ecotone in northeastern China driven by spring temperature and tree cover

Chao Ding [a], Wenjiang Huang [b,*], Shuang Zhao [c], Biyao Zhang [b], Yao Li [d], Fang Huang [e], Yuanyuan Meng [f]

[a] Center for Territorial Spatial Planning and Real Estate Studies, Beijing Normal University at Zhuhai 519087, China
[b] Key Laboratory of Digital Earth Science, Aerospace Information Research Institute, Chinese Academy of Sciences, Beijing 100094, China
[c] School of Geology and Geomatics, Tianjin Chengjian University, Tianjin 300384, China
[d] Zachry Department of Civil and Environmental Engineering, Texas A&M University, College Station, TX 77843, United States of America
[e] School of Geographical Sciences, Northeast Normal University, Changchun 130024, China
[f] Institute of Ecology, College of Urban and Environmental Sciences and Key Laboratory for Earth Surface Processes of the Ministry of Education, Peking University, Beijing 100871, China

ARTICLE INFO

Keywords:
Land surface phenology
Forest-grassland ecotone
Greenup date
Trend
Percent tree cover
Spring warming
MODIS time series

ABSTRACT

Changes in climate and land cover are potential drivers of land surface phenology changes. Here, we investigate whether subpixel percent tree cover (PTC) change is an important driver of trends in satellite derived vegetation spring greenup date (GUD) across the Hulunbuir temperate forest-grassland ecotone in northeastern China. GUD was estimated using the MODIS-derived enhanced vegetation index time series during 2001–2020 with a spatial resolution of 500 m. To understand the influential mechanisms of PTC on GUD, we examined relationships between the spatial variations in GUD and PTC at multiple spatio-temporal extents. Forested pixels with greater PTC were found to have generally earlier GUDs for all forest types. The GUD of forests was also generally earlier than that of grassland. On the other hand, we observed approximately 23.7% and 1.2% significantly earlier and later trends in GUD across the region, respectively. Meanwhile, widespread increases in preseason land surface temperature (LST) and PTC were detected. Both increases in LST and PTC contributed to the earlier GUD in the forested region. Specifically, we found negative correlations (Spearman correlation coefficient -0.17 to -0.55) between the change slopes of GUD and PTC in every forest and grassland type. The results highlight the important impacts of subpixel PTC on GUD variations, and improve the understanding of ecosystem changes under the effects of climate and human activities (e.g., afforestation) over the Hulunbuir temperate forest-grassland ecotone.

1. Introduction

Changes in land surface phenology (LSP), which are derived from satellite remote sensing time series, offer a critical perspective for understanding vegetation and landscape dynamics under environmental changes over large scales (Reed et al., 2009; Henebry and de Beurs, 2013; Piao et al., 2019). In recent decades, many studies have reported LSP changes and the drivers (e.g., Tucker et al., 2001; Jeong et al., 2011; Jeganathan et al., 2014; Garonna et al., 2016). It has been well accepted that changes in climate and land cover/vegetation structure are potential drivers of LSP changes (de Beurs and Henebry, 2004; White et al., 2005; Jeganathan et al., 2014; Zhang et al., 2019), as satellite time series observations capture vegetation dynamics within a landscape (Henebry and de Beurs, 2013; Guan et al., 2014; Helman et al., 2018).

Although most LSP studies have focused on climate drivers, previous studies have highlighted the influences of land cover or vegetation structure on the spatio-temporal dynamics of LSP across diverse ecosystems across spatial scales. In agricultural areas, de Beurs and Henebry (2004) showed that LSP changes characterized by the growing degree days model in Kazakhstan were affected by land use change induced by the collapse of the Soviet Union. Changes in crop types and agricultural management also contributed greatly to the temporal variation in LSP in recent decades across the USA (Zhang et al., 2019; Liang et al., 2021). With regard to savannas, the effects of tree cover and

* Corresponding author.
E-mail addresses: dingchao@bnu.edu.cn (C. Ding), huangwj@aircas.ac.cn (W. Huang).

https://doi.org/10.1016/j.agrformet.2021.108780
Received 23 August 2021; Received in revised form 25 October 2021; Accepted 13 December 2021

tree grass ratio on the spatial patterns of LSP have been observed (Ma et al., 2013; Guan et al., 2014; Cho et al., 2017). For example, Cho et al. (2017) revealed significant spatial differences in phenological metrics among different tree cover levels across southern African savannas. Tree cover has also been identified as an important factor affecting LSP in some forested regions in the Northern Hemisphere (Jeganathan et al., 2014; Misra et al., 2018; Wang et al., 2021). Jeganathan et al. (2014) showed that an earlier start of growing season was associated with a strong loss in fractional forest cover. Wang et al. (2021) reported that the ratio of trees to vegetation impacted the spatio-temporal patterns of LSP in New Mexico, USA. In addition, spring greenup date in shrublands was found to be related to the percent of shrub and herbaceous vegetation cover (Peng et al., 2021).

The Hulunbuir forest-grassland ecotone located in northeastern China is a typical mid-high latitude temperate ecotone. The ecotone has multiple key ecosystem functions and services, such as hydrological regulation and biodiversity conservation (Lv et al., 2012). Understanding the drivers of LSP changes can improve the evaluation and monitoring of ecosystem functions and services for this region (Reed et al., 2009). As an ecologically sensitive area, ongoing changes in land cover or vegetation composition have been observed under various impacts of natural and anthropogenic factors, such as climate variability, fires and afforestation (Gao et al., 2009; Lv et al., 2012; Wang et al., 2013; Ma et al., 2016; Mackenzie et al., 2021). For example, Gao et al. (2009) reported a decrease in tree crown density and a shift toward drought-tolerant understory vegetation in this region between 1988 and 2006. Specifically, large-scale forest management, for instance, tree harvesting and tree planting, as well as cultivation activities, have led to widespread land use and land cover changes, particularly tree cover changes, in recent decades (Lv et al., 2012; Yu et al., 2015; Huang et al., 2018). Tree cover changes were also observed by satellite data (Jia et al., 2015; Chen et al., 2019). In the meanwhile, recent LSP studies revealed earlier spring vegetation greenup over this region, and the climate drivers were also illustrated (e.g., Hou et al., 2018; Wu et al., 2021). However, to the best of our knowledge, the influences of tree cover on LSP changes across this ecotone are still unclear.

Here, we aim to investigate whether tree cover changes play an important role in the changes in spring vegetation greenup date (GUD) across the Hulunbuir forest-grassland ecotone during the last two decades (2001–2020). We used Moderate Resolution Imaging Spectroradiometer (MODIS) time series to estimate GUD, and characterized linear trends in GUD. Changes in tree cover and spring temperature were also analyzed. We then analyzed how tree cover changes influence GUD changes.

2. Data and methods

2.1. Study area

The study area is a forest-grassland ecotone in Hulunbuir, Inner Mongolia, northeastern China (Fig. 1a). Located in the mid-high latitudes of eastern Eurasia, this region has a temperate monsoon climate. The region shows diverse land cover types along with a climate gradient (Fig. 1b). The land cover map in Fig. 1b was obtained from the Copernicus Global Land Service (CGLS) collection 3 land cover product (100 m spatial resolution) for 2015 (Buchhorn et al., 2020; https://lcviewer.vito.be/2015). In terms of the leaf type of forests, the CGLS land cover product includes six types, and each leaf type has closed and open subtypes. For each leaf type, we combined the closed and open subtypes to ensure a sufficient tree cover gradient to investigate the spatial relationships between GUD and subpixel tree cover. Deciduous needleleaf, deciduous broadleaf, and unknown leaf types account for more than 99% of the forests. Forests with other leaf types were therefore excluded from our analysis. We projected the land cover map to a 500 m spatial resolution using the resampling technique of the majority. Deciduous needleleaf forest is the most widespread forest type, and is mainly located in the north of the region. The majority of deciduous broadleaf forest and cropland are distributed in the eastern and western sides of the Greater Khingan Mountains. The spatial distribution of unknown forest is fragmented. Most of the unknown forest are located in the

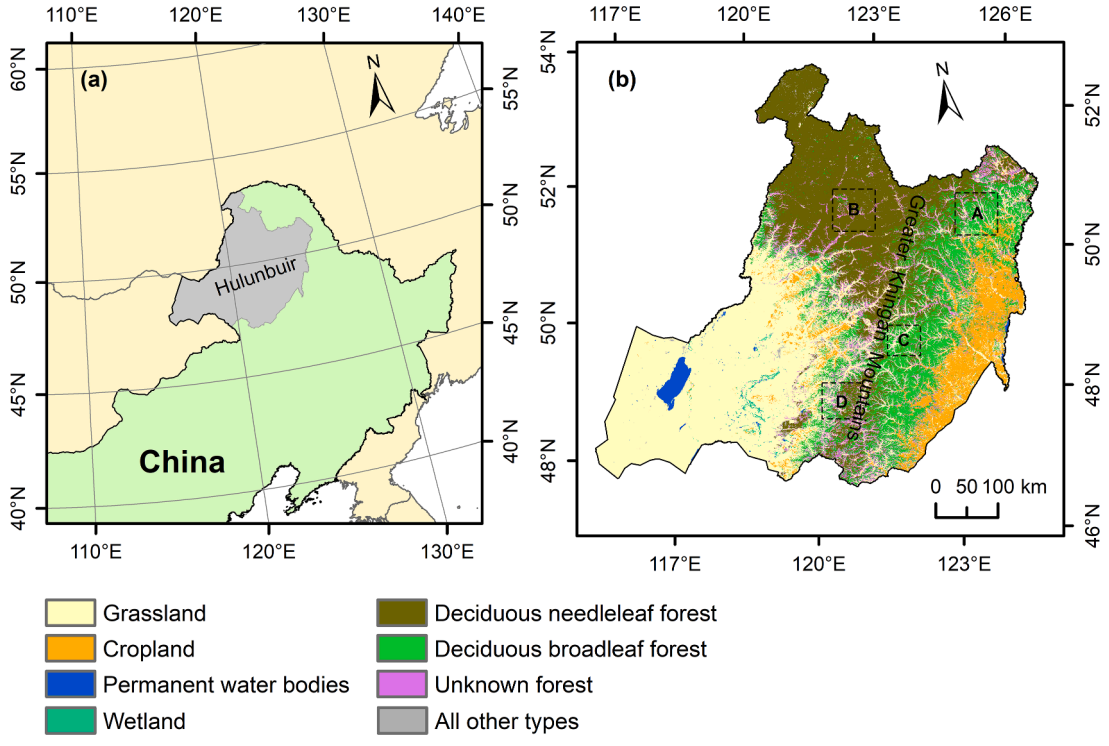

Fig. 1. Land cover map with a 500 m spatial resolution of the Hulunbuir forest-grassland ecotone in northeastern China for 2015 derived from the Copernicus Global Land Service (CGLS) collection 3 land cover product.

transition areas among land cover types. Grassland and wetland mainly exist in the western part of this ecotone. The change analysis on GUD was performed for the major land cover types, including deciduous needleleaf forest, deciduous broadleaf forest, unknown forest, grassland, and cropland.

2.2. Datasets

2.2.1. MODIS surface reflectance data

We obtained the Terra/MODIS Collection 6 MOD09A1 8-day composite reflectance data with a spatial resolution of 500 m (Vermote, 2015) for the 2001–2020 period from https://ladsweb.modaps.eosdis.nasa.gov/. The enhanced vegetation index (EVI, Huete et al., 2002) was selected for the estimation of GUD. In this mid-high latitude region, seasonal snow cover dynamics can affect the seasonal EVI patterns (Shabanov et al., 2002; Delbart et al., 2005). Thus, we also used the normalized difference snow index (NDSI, Hall et al., 1995) to track snow cover dynamics. We calculated the EVI and NDSI as follows:

$$EVI = 2.5 * \frac{\rho_{NIR} - \rho_{red}}{\rho_{NIR} + 6 * \rho_{red} - 7.5 * \rho_{blue} + 1} \quad (1)$$

$$NDSI = \frac{\rho_{green} - \rho_{SWIR}}{\rho_{green} + \rho_{SWIR}} \quad (2)$$

where ρ_{red}, ρ_{NIR}, ρ_{blue}, ρ_{green}, and ρ_{SWIR} are the reflectance of red (band 1 of MOD09A1), near infrared (band 2), blue (band 3), green (band 4), and shortwave infrared (band 6) bands, respectively.

2.2.2. Tree cover data

The annual tree cover data were provided by the MODIS MOD44B Collection 6 vegetation continuous field product at 250 m spatial resolution (Townshend et al., 2015). We obtained the MOD44B data during 2001–2020 from https://search.earthdata.nasa.gov/search. This product uses both MODIS optical and thermal infrared bands as inputs, and provides the annual subpixel percent tree cover (PTC, tree canopy height $\geq$ 5 m), non-tree vegetation, and bare area (Townshend et al., 2015; DiMiceli et al., 2021). This product has been widely used to quantify long-term changes in tree cover (e.g., Song et al., 2014; Chen et al., 2019). We resampled the 250 m PTC to 500 m using bilinear interpolation.

2.2.3. Land surface temperature data

We used land surface temperature (LST) derived from the Terra/MODIS MOD11A2 Collection 6 product (Wan et al., 2015), which has an 8-day temporal interval and 1000 m spatial resolution, as the major climate driver of GUD changes. The MOD11A2 data from 2001 to 2020 were obtained from https://ladsweb.modaps.eosdis.nasa.gov/. Many studies have shown strong correlations between surface air temperature and MODIS-derived LST across the globe and northeastern China (e.g., Janatian et al., 2017; Zhu et al., 2017; Yang et al., 2017). Furthermore, strong spatio-temporal links between MODIS-derived LST and spring phenology have been observed in diverse ecosystems (Zhang et al., 2004; Hanes and Schwartz, 2011; Hou et al., 2018; Tomaszewska and Henebry, 2020). The spatial resolution of the MOD11A2 LST product allows to capture the spatial differences in temperature and its temporal variations within small regions. The LST data were therefore selected to attribute drivers of spring phenology in this mountainous forest-grassland ecotone that exhibits spatially heterogeneous temperature patterns. We identified and removed all poor quality observations in the LST data using the quality assurance layer and filled the gaps in the daytime and nighttime LST time series using linear interpolation (Zhang et al., 2015). We then generated the average LST time series based on the daytime and nighttime observations and resampled the average LST to a 500 m resolution using bilinear interpolation.

2.3. Estimation of GUD

We first identified and removed observations contaminated by clouds and cloud shadows in the 8-day interval EVI time series using the state quality assurance layer included in the MOD09A1 product. We then identified observations with a NDSI value greater than 0.1 as snow. This NDSI threshold was set according to Gladkova et al. (2012). We replaced snow observations in the EVI time series using the 5th quantiles of all clear observations in the current and next years following Gray et al. (2019). Cloudy observations in the EVI time series were then filled using linear interpolation. We finally modeled the EVI time series using the Asymmetric Gaussians function fitting (Jönsson and Eklundh, 2002). This fitting process was implemented in the TIMESAT 3.3 software (Jönsson and Eklundh, 2004; Eklundh and Jönsson, 2017). Before performing the Asymmetric Gaussians fitting, we selected the median filtering to further reduce abnormal values in the EVI time series. The spike value of the median filtering was set as 0.5. We fitted the upper envelope of the EVI time series with an iteration times of 3 and adaption strength of 2. GUD was estimated using the threshold of the 20% of the seasonal EVI amplitude. Less than 0.01% of the pixels had more than one growing cycles in one year, and these pixels were removed. The TIMESAT software may fail to extract the GUD of some pixels due to poor data quality, and these pixels were not considered in the following analysis. Furthermore, we also excluded pixels with GUD before day of year 90. In this case, GUD was regarded as an abnormal value according to our prior knowledge of the study region.

2.4. Statistical analysis

2.4.1. Relationships between GUD and subpixel PTC

To understand how subpixel PTC influences satellite observed GUD in this forest-grassland ecotone, we examined the relationships between the spatial patterns of GUD and PTC across spatial and temporal scales. The Spearman rank correlation coefficients between the temporal mean GUD and PTC for the 2001–2020 period were calculated across the whole study region and several subregions for each forest type. For the whole study region, the analysis was performed based on 5% random samples across the region (de Beurs et al., 2015; Wang et al., 2021). We selected four subregions with strong spatial variations in PTC, as shown in Fig. 1b and Fig. S1. Subregions A, C, and D were selected for deciduous broadleaf forest and unknown forest, and subregion B for deciduous needleleaf forest. Although subregion D also contains a large proportion of deciduous needleleaf forest, this subregion was not analyzed for deciduous needleleaf forest because its spatial variation in PTC was small. Furthermore, the spatial differences in spring temperature also affect the spatial pattern of GUD. We also calculated the Spearman rank partial correlation coefficient between the mean GUD and PTC by controlling the spring mean LST (day of year 97–128). For a spatial comparison, it is reasonable to use LST with the same period to reflect which pixels were warmer than others.

In addition to the analysis of multiyear mean GUD and PTC, we also analyzed the spatial relationship between GUD and PTC for each year to further understand the uncertainties. Furthermore, the GUD of forests and grassland was also compared for each year. If impacts of subpixel PTC on GUD spatial variations were observed, then temporal changes in PTC can be a potential driver of temporal changes in GUD in theory.

2.4.2. Temporal changes in GUD and the potential drivers

A variety of studies have demonstrated that temporal variation in GUD is related to preseason temperature variation across the temperate region of China (e.g., Piao et al., 2006; Chen et al., 2012). Here, we calculated the preseason mean LST with a preseason length of 24 days (i.e., three 8-day composite periods). For each pixel, the last 8-day composite period of the preseason was determined by its multiyear mean GUD (Liu et al., 2016). We also tested the preseason length of 32 days and 40 days, and the Spearman correlation coefficients between the

GUD and LST time series were similar to that of the preseason length of 24 days (Fig. S2).

We estimated linear changes in GUD, preseason mean LST, and PTC during 2001–2020 using the Theil-Sen slope (Sen, 1968; Theil, 1992) and tested the significance of change by the Mann-Kendall test (Mann, 1945). Specifically, grassland with a mean PTC during 2001–2020 smaller than 10% and cropland were excluded from the PTC change analysis. Note that the land cover map (Fig. 1b) represents the dominant land cover type within a 500 $m\times$ 500 m pixel; hence, grassland pixels can also contain trees (i.e., mixed pixels) in this forest-grassland ecotone with heterogeneous landscapes. The threshold of 10% was set to exclude grassland pixels with very low tree cover throughout the study period, and for these pixels PTC change may not be a driver of GUD changes. In total, PTC change analysis was performed for 20.6% of the grassland pixels.

To investigate the potential drivers of GUD changes, we classified pixels with significant GUD trends into several types based on trend combinations of preseason mean LST and PTC. Different types could indicate different potential drivers of GUD trends. We further examined the Spearman rank correlations between the change slopes (Theil-Sen slopes) of GUD and PTC for each land cover type for 5% random pixels across the whole study region and for three subregions. The three subregions were used as examples to illustrate the influences of PTC changes on GUD, and were delineated in areas showing a spatially continuous GUD change type, i.e., significantly earlier GUD with only significant increase in PTC.

3. Results

3.1. Spatial difference in GUD under different subpixel PTC levels

The spatial relationships between the mean GUD and PTC during 2001–2020 of deciduous broadleaf forest are provided in Fig. 2. A negative correlation (r=−0.43) between GUD and PTC was found across the whole study region (Fig. 2a, Table 1). Much stronger negative correlations were revealed in the subregions. Moreover, negative correlations were also found for all 20 years with different meteorological conditions, although the correlation coefficients were weak in some years, especially for the whole study area and subregion A. For subregions C and D, strong negative correlations ($r<-0.5$) were observed for more than ten years. Negative correlations were also found in deciduous needleleaf forest (Fig. 3) and unknown forest (Fig. 4). A positive but very weak correlation ($r<0.1$) occurred in 2004 for deciduous needleleaf forest (Fig. 3d). Furthermore, most of the partial correlation coefficients between GUD and PTC by controlling spring LST were strongly negative (Table 1). Overall, the negative correlations between GUD and PTC indicated that in the forested region, pixels with higher PTC generally had earlier GUD. In addition, the GUDs of forests were also earlier than that of grassland for most years (Fig. 5). The differences in GUD between grassland and forests were more evident for the grassland that is spatially adjacent to forests (Fig. S1).

3.2. Changes in GUD during 2001–2020

Changes in GUD across the Hulunbuir forest-grassland ecotone for the period 2001–2020 are presented in Fig. 6a. Overall, approximately 23.7% of the region experienced significantly earlier trends in GUD ($p \leq 0.05$, Table 2). Deciduous broadleaf forest and unknown forest showed the strongest mean change slopes. The spatial patterns of significantly earlier GUD of grassland and deciduous broadleaf forest were spatially clustered. For grassland, significantly earlier GUD mainly occurred in the eastern part, which is adjacent to the forested region. Many grassland pixels showed GUD advancement by greater than 0.75 days/year. Most of the significantly earlier GUD for deciduous broadleaf forest were distributed in the northeastern part, with absolute rates of change greater than 0.5 days/year. Significantly earlier GUD of deciduous needleleaf forest was observed mainly in the central and northern regions. Significantly later GUD were observed for only approximately 1.2% of the region, of which most were distributed in the western grassland and eastern cropland regions.

3.3. Changes in preseason LST and PTC during 2001–2020

Fig. 6b presents the changes of the preseason LST. We observed

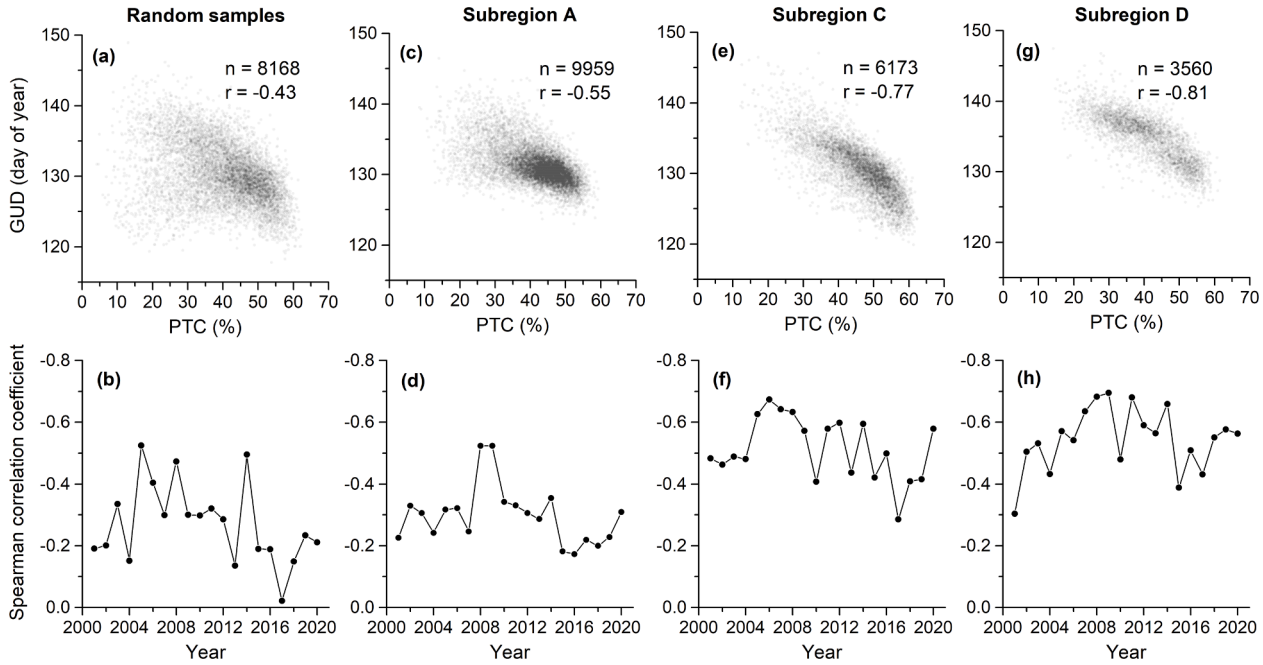

Fig. 2. Relationship between the mean greenup date (GUD) and percent tree cover (PTC) during 2001–2020 and the Spearman correlation coefficient between GUD and PTC for each year of deciduous broadleaf forest. (a) (b) Random samples selected from the whole region, (c) (d) subregion A, (e) (f) subregion C, and (g) (h) subregion D. All correlation coefficients were statistically significant ($p \leq 0.05$).

Table 1
Correlations between the spatial variations of the mean greenup date (GUD) and percent tree cover (PTC) during 2001–2020. r, Spearman correlation coefficient; pr, Spearman partial correlation coefficient by controlling the mean spring land surface temperature.

Forest type	Random samples		Subregion A		Subregion B		Subregion C		Subregion D	
	r	pr	r	pr	r	pr	R	pr	r	pr
Deciduous broadleaf forest	−0.43	−0.62	−0.55	−0.59	–	–	−0.77	−0.77	−0.81	−0.82
Deciduous needleleaf forest	−0.36	−0.39	–	–	−0.50	−0.61	–	–	–	–
Unknown forest	−0.31	−0.59	−0.58	−0.64	–	–	−0.81	−0.78	−0.81	−0.84

Note: all correlation coefficients were statistically significant ($p \leq 0.05$).

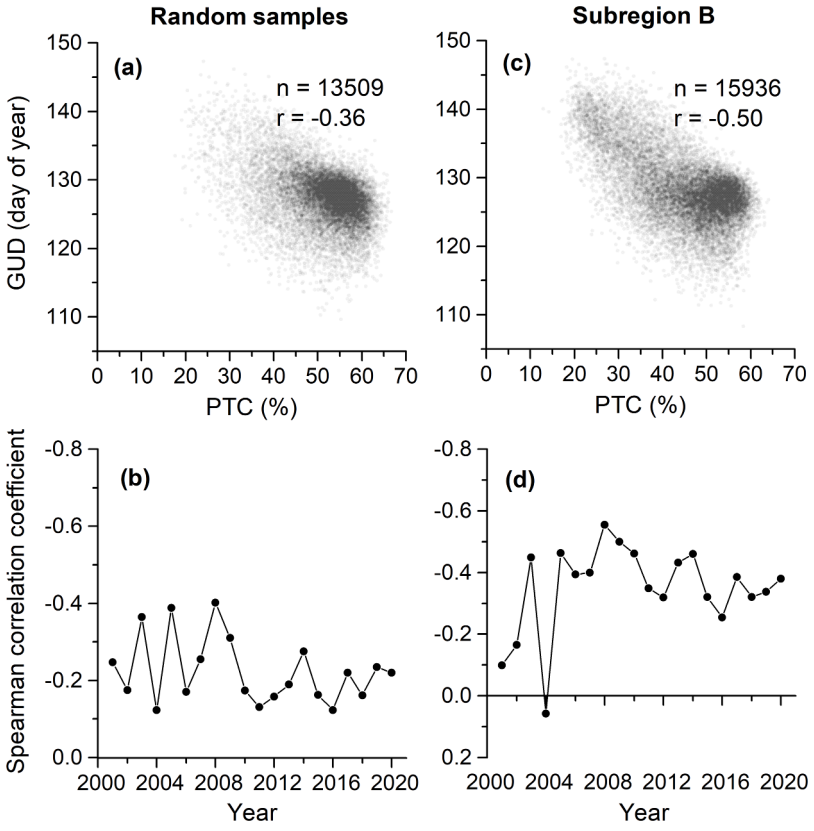

Fig. 3. Relationship between the mean GUD and PTC during 2001–2020 and the Spearman correlation coefficient between GUD and PTC for each year of deciduous needleleaf forest. (a) (b) Random samples selected from the whole region and (c) (d) subregion B. All correlation coefficients were statistically significant ($p \leq 0.05$).

significant increases in preseason LST for approximately 46.2% of the region (111,204 km^2). Most of the warming regions had a slope greater than 0.1 °C/year. The strongest increase in spring temperature was found in the central region, i.e., the forested region in the Greater Khingan Mountains. A small area of significantly cooling preseason was observed in the southeastern region.

The spatial distribution of PTC changes is presented in Fig. 6c. In total, a significant increase in PTC was observed for approximately 41.5% of the analyzed region. All land cover types showed large proportions of significant PTC increase (Table 3). Among the land cover types, unknown forest showed the greatest mean PTC increase, followed by grassland and deciduous broadleaf forest. Strong tree cover increases were mainly distributed in the west and northeast of the forested region. Only about 2.4% of the region showed significantly decreased PTC. Most of these PTC decreases occurred in deciduous needleleaf forest in the northern region.

3.4. Influences of preseason LST and PTC on GUD temporal changes

Significantly earlier GUDs ($p \leq 0.05$) were classified into five types according to the trend combinations of preseason LST and PTC (Fig. 7). Areas with significantly later GUD trends were not considered because they accounted for a very small proportion of the region. In total, approximately 26.6% of the significantly earlier GUD corresponded to only a significant increase in preseason LST (Type 1, Table 4). As interannual variations in GUD generally showed negative correlations with preseason LST in the forested region (Fig. S2), the increases in LST were likely to be the major driver of earlier GUD for Type 1. With regard to land cover types, Type 1 accounted for large proportions of the deciduous broadleaf forest and deciduous needleleaf forest (Table 4). A large patch of Type 1 was observed in the deciduous broadleaf forest in the southeastern region. For the Type 2 case, both preseason LST and PTC showed significant increases, and GUD changes may be driven by both of the two factors. Increases in PTC may be the major driver of earlier GUD for Type 3, which showed the greatest proportion (36.0% in total) among the five types. Large proportions (>50%) of Type 3 were found in unknown forest and grassland. Subregions I, II and III in Fig. 7 are typical regions with spatially continuous Type 3. For a stricter significance level (α=0.01), we found the proportion of Type 3 was much greater than that of Type 1 (Table S1). Overall, most significantly earlier GUD were associated with significant increases in LST and/or PTC, and approximately 18.0% showed non-significant trends in LST and PTC

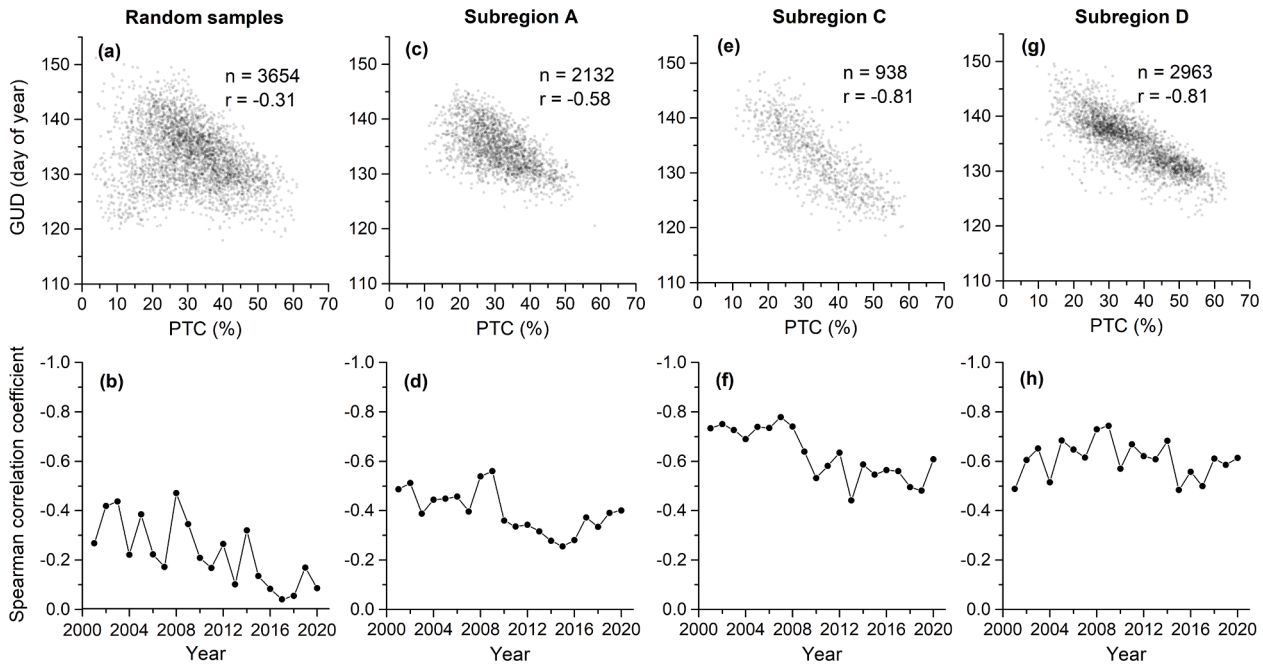

Fig. 4. Relationship between the mean GUD and PTC during 2001–2020 and the Spearman correlation coefficient between GUD and PTC for each year of unknown forest. (a) (b) random samples selected from the whole region, (c) (d) subregion A, (e) (f) subregion C, and (g) (h) subregion D. All correlation coefficients were statistically significant ($p \leq 0.05$).

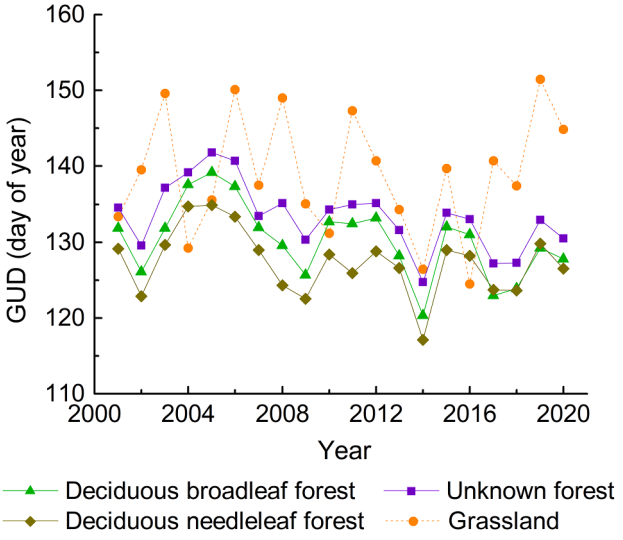

Fig. 5. Comparison of regional mean GUD between forests and grassland.

(Type 4). Other cases (Type 5) had a very small proportion.

The relationships between the change slopes of GUD and PTC for the three subregions with spatially continuous Type 3 and the whole study region further illustrate the role of PTC in advancing GUD (Fig. 8). As expected, negative correlations between GUD and PTC slopes were revealed for all land cover types in different subregions, after masking out the pixels with Types 1 and 4 that were not likely to be affected by PTC. Pixels with greater PTC increases generally had greater advances in GUD. This phenomenon was more obvious in deciduous broadleaf forest and unknown forest (Fig. 8).

4. Discussion

4.1. Spatial difference in GUD in relation to subpixel PTC

PTC of a pixel or landscape was observed to affect its GUD, i.e., pixels with greater tree cover generally had earlier GUDs (Figs. 2-4). The observed GUD and PTC relationships could be mainly explained by the generally earlier GUD of tree species than that of herbaceous species across this temperate forest-grassland ecotone. In this region, a 500 $m\times$ 500 m pixel in the transition zone of forest and grassland may be a mosaic of patches of forest and grassland. Using a simulation method with MODIS NDVI time series of temperate forest and cropland end-members in northeastern China, Chen et al. (2018) illustrated that an increase in the percentage of forest in a pixel leads to an advance in GUD. In Chen et al. (2018), the forest endmember has an earlier GUD and a greater seasonal NDVI amplitude than those of the cropland endmember. In this study, the GUDs of forests were generally earlier than that of grassland as shown in Fig. 5. Deciduous forests also have greater seasonal EVI amplitude than grassland. Similar to the mixed pixel effect of forest and cropland in Chen et al. (2018), it is reasonable to infer that pixels with a greater percentage of tree canopy had greenup that occurred earlier, especially in mosaic landscapes of forest and grassland. According to these results, tree cover increases over time are expected to induce a trend toward earlier GUD.

Uncertainties of the relationships between GUD and PTC may occur within the forested region, where some understory species may turn green earlier in spring than the overstory trees to use the light, i.e., the phenological escape phenomena (Richardson and O'Keefe, 2009). Earlier understory greenup has been reported in many temperate deciduous forests in North America (e.g., Ahl et al., 2006; Richardson and O'Keefe, 2009) and Europe (e.g., Berra et al., 2019; Calders et al., 2015; Doktor et al., 2009; Pisek et al., 2015). In this forest-grassland ecotone, the overstory canopy cover (i.e., tree canopy higher than 5 m) is generally sparse. The mean PTC in 2001–2020 was mostly lower than 60% (Fig. S1b). Hence, the phenological escape phenomena might not be obvious in major understory species across this region, and this needs further investigation. Berra et al. (2019) also reported later understory

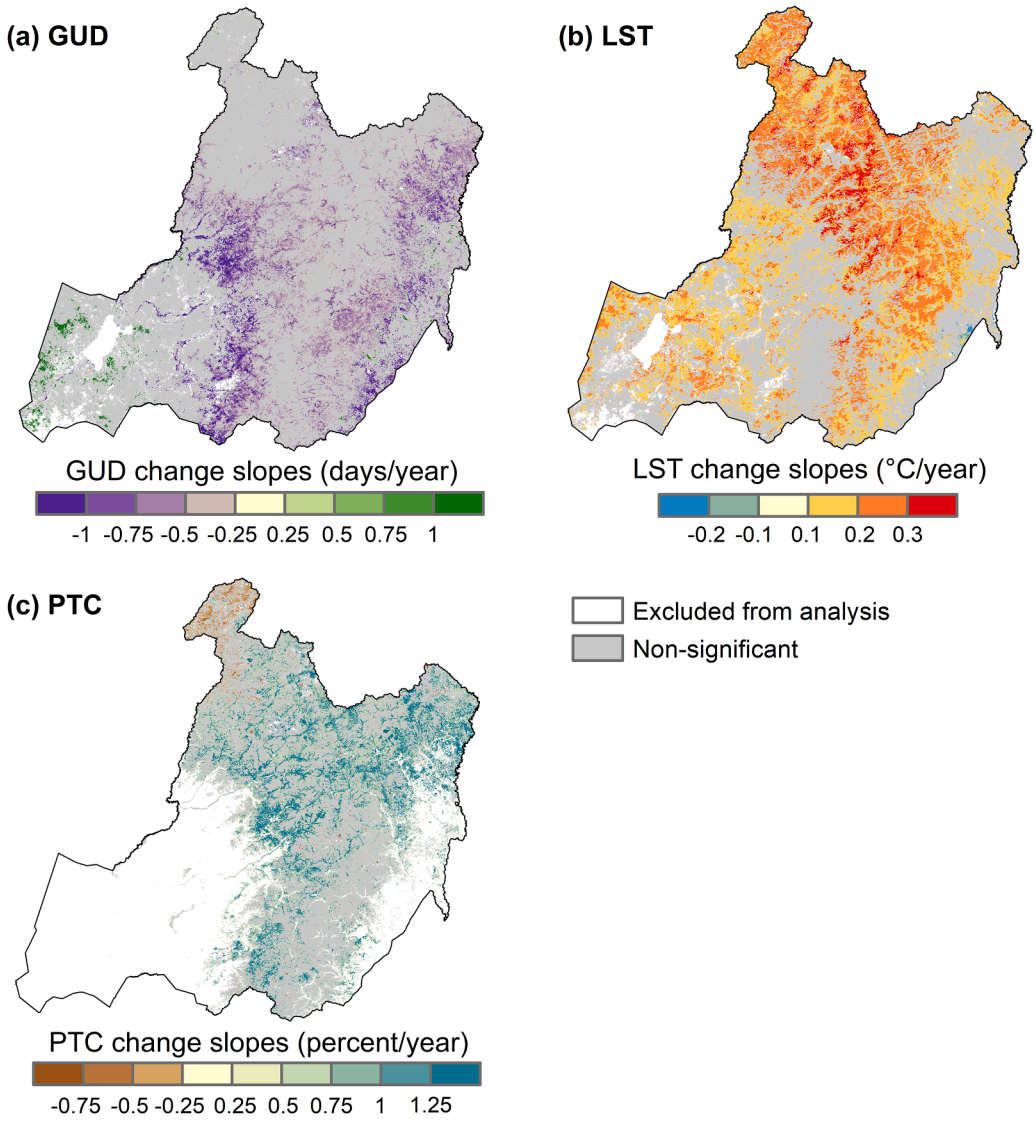

Fig. 6. Changes in (a) GUD, (b) preseason mean land surface temperature (LST), and (c) PTC during 2001–2020 across the Hulunbuir forest-grassland ecotone.

Table 2
Statistics of GUD changes during 2001–2020 for different land cover types.

Land cover type	Significantly earlier GUD (%)	Significantly later GUD (%)	Mean Slope (days/year)	Standard deviation of slope
Deciduous broadleaf forest	33.1	<0.1	−0.41	0.17
Deciduous needleleaf forest	13.1	0.2	−0.25	0.22
Unknown forest	37.2	0.1	−0.41	0.24
Grassland	24.3	2.4	−0.02	0.90
Cropland	24.8	2.1	−0.33	0.47
Total	23.7	1.2	−0.21	0.61

Note: the significance level is α=0.05.

Table 3
Statistics of PTC changes during 2001–2020 for different land cover types. For grassland, the statistics were computed for only pixels with mean PTC during 2001–2020 greater than 10%.

Land cover type	Significant increase (%)	Significant Decrease (%)	Mean Slope (%/year)	Standard deviation of slope
Deciduous broadleaf forest	38.3	0.3	0.55	0.50
Deciduous needleleaf forest	34.0	4.6	0.36	0.50
Unknown forest	57.2	0.5	0.70	0.51
Grassland	60.5	0.8	0.60	0.47
Total	41.5	2.4	0.49	0.52

Note: the significance level is α=0.05.

development in a sparse forest.

Other factors can also partially explain the uncertainties. For example, the sensitivities of phenological metrics to fractional cover change of different tree species may be different, as shown in Misra et al. (2018). Furthermore, the scaling effects of mixed pixels can influence the GUD and PTC relationships (Chen et al., 2018; Peng et al., 2017; Zhang et al., 2017). Zhang et al. (2017) suggested that in a mixed pixel, earlier greenup vegetation contributed disproportionately to the estimated GUD. We analyzed the GUD and PTC relationships for each forest

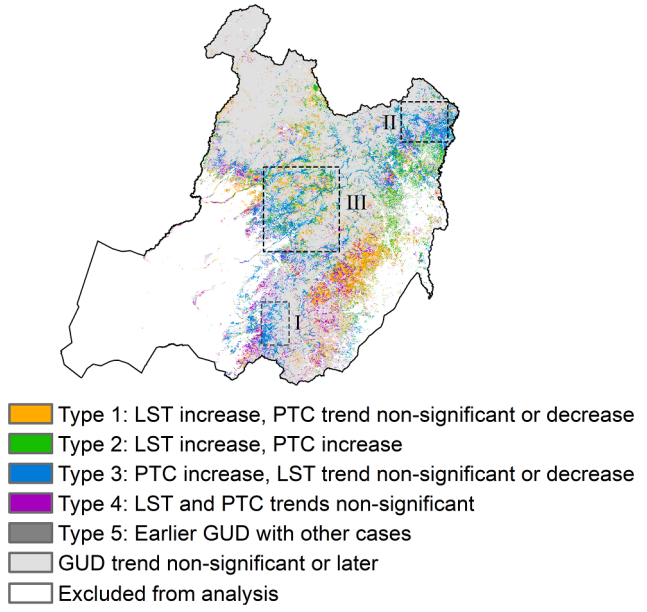

Fig. 7. Significantly earlier GUD with different trend combinations of preseason LST and PTC.

Table 4
Percentage of significantly earlier GUD ($p \leq 0.05$) with different trend combinations of preseason LST and PTC for each land cover type. The description of the types is provided in Fig. 7.

Land cover type	Type 1	Type 2	Type 3	Type 4	Type 5
Deciduous broadleaf forest	35.1	20.4	24.7	19.8	0.0
Deciduous needleleaf forest	39.2	25.6	22.5	12.4	0.3
Unknown forest	14.7	18.8	50.5	16.0	0.0
Grassland	11.5	12.2	54.2	22.0	0.1
Total	26.6	19.3	36.0	18.0	0.1

type and for different subregions to reduce the uncertainties. And we have shown the general influences of PTC on GUD (i.e., negative correlation) from the perspective of spatial variation. Indeed, the influences of PTC on GUD are the results of mixed pixels, and a quantitative evaluation of the scaling effects across this ecotone is needed to further understand the GUD and PTC relationships.

4.2. Trends in GUD and the drivers

We observed a significantly earlier GUD ($p \leq 0.05$) for approximately 23.7% of the Hulunbuir forest-grassland ecotone during 2001–2020 (Table 2). A large area of the significant trend of earlier GUD was found in deciduous broadleaf forest and unknown forest. The spatial pattern of GUD changes was generally similar to the results in previous studies covering similar time periods (e.g., Hou et al., 2018; Wu et al., 2021). However, differences in GUD slopes compared with previous studies were also found, partially due to differences in the satellite datasets, vegetation indices, and definitions of GUD (White et al., 2009).

It has been well accepted that an increase in spring temperature generally causes an advance in the GUD of forests in northern mid-high latitude regions (e.g., Tucker et al., 2001; Menzel et al., 2006; Jeong et al., 2011). Hou et al. (2018) showed that increases in spring temperature can lead to advances in vegetation greenup during 2001–2016 in northeastern China. In this ecotone, the interannual variations in GUD for most forested pixels were negatively correlated with the preseason mean LST (Fig. S2). Widespread increases in preseason mean LST were observed during the study period (111,204 km^2, Fig. 6b). This warming spring could partially explain the earlier GUD. Many pixels with significantly earlier GUD were associated with increased LST (Fig. 7, Table 4).

The forested region experienced an apparent PTC increase (Fig. 6c). A similar spatial pattern of PTC change was also observed by Chen et al. (2019), who evaluated tree cover change in China using the MODIS vegetation continuous field data of 2000–2002 and 2014–2016 at a 0.05° spatial resolution. For a longer period, Jia et al. (2015) analyzed changes in fractional forest cover over Northeast China during 1982–2011. In Jia et al. (2015), the Global Inventory Modeling and Mapping Studies (GIMMS3g) dataset was applied to calculate the subpixel fractional forest cover. Widespread increases and decreases in forest cover were found in Hulunbuir, and the observed forest cover changes were generally not significantly correlated with variations in either temperature or precipitation (Jia et al., 2015). In recent two decades, the PTC increase across this forest-grassland ecotone may be primarily explained by afforestation and young forest growth under several ecosystem protection projects (Liu et al., 2008; Jia et al., 2015; Chen et al., 2019), such as the Natural Forest Conservation Program (Liu et al., 2008). As discussed in Section 4.1, PTC change can be a potential driver of GUD change. A large proportion of pixels showing significantly earlier GUD was associated with significantly increased PTC (Table 4). The negative correlations between the change slopes of GUD and PTC further confirmed the influences of increased PTC on the earlier GUD (Fig. 8). It is worth noting that climate variations can affect young forest growth, and therefore climate may also have indirect impacts on the observed GUD changes. But in this study, we focus on the direct impacts of climate (i.e., temperature) and tree growth on GUD changes. Overall, our results highlight that in addition to the spring warming, the increase in tree cover was also an important factor that contributed to the earlier GUD across Hulunbuir in recent two decades.

For grassland with very low PTC, which account for most grassland in the region, previous studies have illustrated the influences of spring temperature and precipitation on GUD variations (e.g., Tang et al., 2015; Ren et al., 2018; Fan et al., 2020). This study focused more on the effects of tree cover change on GUD, and we therefore did not further investigate the climate drivers of the GUD trend in grassland.

Our analysis highlights the importance of subpixel PTC change in the earlier GUD over the Hulunbuir temperate forest-grassland ecotone. However, we also observed some areas with tree cover increases but exhibited small changes in GUD, which mainly occurred in deciduous needleleaf forest. This suggests the complexities of LSP changes in response to tree cover change or the influences of other climate or non-climate factors on GUD. For example, fires and natural community succession may also contribute to GUD changes, and may partially explain the uncertainties of GUD drivers (Zhang et al., 2019; Tong et al., 2019; Wu et al., 2021). Changes in the start of the growing season induced by fire events across the Mongolian Plateau have been observed by Wu et al. (2021). In addition, topography may also affect GUD and its response to PTC, because topography, especially deep terrain, can lead to strong differences in climatic conditions within a small region (Hwang et al., 2011; An et al., 2018; Tomaszewska et al., 2020).

This study evaluated the qualitative relationship between changes in GUD and tree cover and spring temperature. It is a challenge to disassemble the contribution of climate and non-climate factors to GUD changes across a large region due to the complex mechanisms of ecosystem changes. Besides the uncertainties in GUD and PTC relationships, there are diverse phenological responses to climate variations among overstory and understory species and at different locations (Tremblay and Larocque, 2001; Richardson and O'Keefe, 2009; Hassan and Rahman, 2013). A simulation method of mixed pixels combined with phenology models as well as machine learning algorithms may improve the quantitative assessment in this region (Chen et al., 2018; Wang et al., 2021).

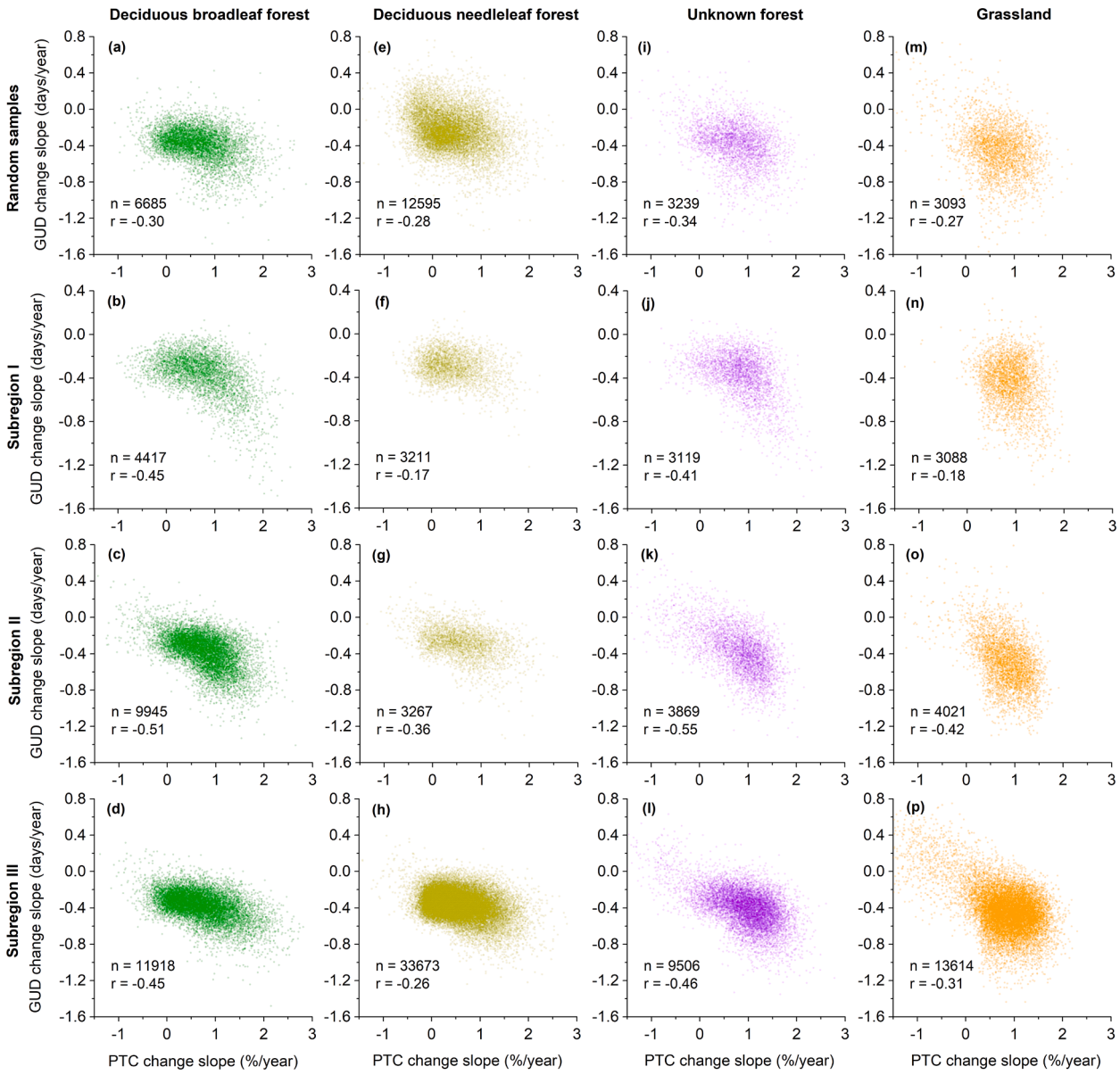

Fig. 8. Spearman correlation coefficients between the slopes of GUD and PTC for different land cover types in different regions. Pixels with Types 1 and 4 changes were masked out. Locations of subregions I, II and III are presented in Fig.7. All correlation coefficients were statistically significant ($p \leq 0.05$).

5. Conclusion

We characterized GUD changes over the Hulunbuir temperate forest-grassland ecotone in northeastern China from 2001 to 2020 under changes in spring temperature and PTC. Spatial differences in GUD in relation to variations in subpixel PTC were observed in the forested region across spatiotemporal scales. Pixel with a greater PTC generally had an earlier GUD, suggesting that PTC increases or decreases may lead to temporal changes in satellite-derived coarse resolution GUDs in this ecotone. With regard to the temporal changes, approximately 23.7% of the region showed significantly earlier GUD trends, while only approximately 1.2% showed a significant delay in GUD. Meanwhile, widespread increases in preseason mean LST and PTC were observed. A combination of trends in GUD, preseason LST, and PTC suggests that both increases in preseason LST and GUD contributed to the earlier GUD in the forested region. Our results highlight the impacts of a non-climate factor (i.e., tree cover) on satellite-observed GUD changes at a coarse spatial resolution across this forest-grassland ecotone. A quantitative assessment of the contributions of changes in tree cover and climate to LSP changes can enhance the understanding of ecosystem processes in the region, which needs further investigation.

Declaration of Competing Interest

The authors declare that they have no known competing financial interests or personal relationships that could have appeared to influence the work reported in this paper.

Acknowledgements

This work was supported by the China Postdoctoral Science Foundation, grant number 2019M660851, and the grant from Beijing Normal University, grant number 310432101. We thank the anonymous reviewers and the editor for their constructive comments on the manuscript.

Supplementary materials

Supplementary material associated with this article can be found, in the online version, at doi:10.1016/j.agrformet.2021.108780.

References

Ahl, D.E., Gower, S.T., Burrows, S.N., Shabanov, N.V., Myneni, R.B., Knyazikhin, Y., 2006. Monitoring spring canopy phenology of a deciduous broadleaf forest using MODIS. Remote Sens. Environ. 104, 88–95.

An, S., Zhang, X., Chen, X., Yan, D., Henebry, G.M., 2018. An exploration of Terrain effects on land surface phenology across the Qinghai-Tibet Plateau using Landsat ETM+ and OLI data. Remote Sens. 10 https://doi.org/10.3390/rs10071069.

Berra, E.F., Gaulton, R., Barr, S., 2019. Assessing spring phenology of a temperate woodland: a multiscale comparison of ground, unmanned aerial vehicle and Landsat satellite observations. Remote Sens. Environ. 223, 229–242. https://doi.org/10.1016/j.rse.2019.01.010.

Buchhorn, M., Smets, B., Bertels, L., Lesiv, M., Tsendbazar, N.-.E., Masiliunas, D., Linlin, L., Herold, M., Fritz, S., 2020. Copernicus Global Land Service: land Cover 100m: collection 3: epoch 2015: globe (Version V3.0.1) [Data set]. Zenodo. https://doi.org/10.5281/zenodo.3939038.

Calders, K., Schenkels, T., Bartholomeus, H., Armston, J., Verbesselt, J., Herold, M., 2015. Monitoring spring phenology with high temporal resolution terrestrial LiDAR measurements. Agric. For. Meteorol. 203, 158–168. https://doi.org/10.1016/j.agrformet.2015.01.009.

Chen, C., Park, T., Wang, X., Piao, S., Xu, B., Chaturvedi, R.K., Fuchs, R., Brovkin, V., Ciais, P., Fensholt, R., Tømmervik, H., Bala, G., Zhu, Z., Nemani, R.R., Myneni, R.B., 2019. China and India lead in greening of the world through land-use management. Nat. Sustain. 2, 122–129. https://doi.org/10.1038/s41893-019-0220-7.

Chen, X., Wang, D., Chen, J., Wang, C., Shen, M., 2018. The mixed pixel effect in land surface phenology: a simulation study. Remote Sens. Environ. 211, 338–344. https://doi.org/10.1016/j.rse.2018.04.030.

Chen, X., Xu, L., 2012. Temperature controls on the spatial pattern of tree phenology in China's temperate zone. Agric. For. Meteorol. 195, 154–155. https://doi.org/10.1016/j.agrformet.2011.11.006.

Cho, M.A., Ramoelo, A., Dziba, L., 2017. Response of land surface phenology to variation in tree cover during green-up and senescence periods in the semi-arid savanna of Southern Africa. Remote Sens. 9. https://doi.org/10.3390/rs9070689.

de Beurs, K.M., Henebry, G.M., Owsley, B.C., Sokolik, I., 2015. Using multiple remote sensing perspectives to identify and attribute land surface dynamics in Central Asia 2001-2013. Remote Sens. Environ. 170, 48–61. https://doi.org/10.1016/j.rse.2015.08.018.

de Beurs, K.M., Henebry, G.M., 2004. Land surface phenology, climatic variation, and institutional change: analyzing agricultural land cover change in Kazakhstan. Remote Sens. Environ. 89, 497–509. https://doi.org/10.1016/j.rse.2003.11.006.

Delbart, N., Kergoat, L., Le Toan, T., Lhermitte, J., Picard, G., 2005. Determination of phenological dates in boreal regions using normalized difference water index. Remote Sens. Environ. 97, 26–38. https://doi.org/10.1016/j.rse.2005.03.011.

DiMiceli, C., Townshend, J., Carroll, M., Sohlberg, R., 2021. Evolution of the representation of global vegetation by vegetation continuous fields. Remote Sens. Environ. 254 https://doi.org/10.1016/j.rse.2020.112271.

Doktor, D., Bondeau, A., Koslowski, D., Badeck, F.W., 2009. Influence of heterogeneous landscapes on computed green-up dates based on daily AVHRR NDVI observations. Remote Sens. Environ. 113, 2618–2632. https://doi.org/10.1016/j.rse.2009.07.020.

Eklundh, L., Jönsson, P., 2017. Timesat 3.3 Software Manual. Lund and Malmö University, Sweden.

Fan, D., Zhao, X., Zhu, W., Sun, W., Qiu, Y., 2020. An improved phenology model for monitoring green-up date variation in Leymus chinensis steppe in Inner Mongolia during 1962-2017. Agric. For. Meteorol. 291, 108091 https://doi.org/10.1016/j.agrformet.2020.108091.

Gao, J.X., Lv, S.H., Liu, J.H., Qiao, Q., Wang, Y.P., Tian, M.R., 2009. Ecological Ecotone in China. China Environmental Science Press, Beijing.

Garonna, I., de Jong, R., Schaepman, M.E., 2016. Variability and evolution of global land surface phenology over the past three decades (1982-2012). Glob. Chang. Biol. 22, 1456–1468. https://doi.org/10.1111/gcb.13168.

Gladkova, I., Grossberg, M., Bonev, G., Romanov, P., Shahriar, F., 2012. Increasing the accuracy of MODIS/Aqua snow product using quantitative image restoration technique. IEEE Geosci. Remote Sens. Lett. 9, 740–743. https://doi.org/10.1109/LGRS.2011.2180505.

Gray, J., Sulla-Menashe, D., Friedl, M.A., 2019. User Guide to Collection 6 MODIS Land Cover Dynamics (MCD12Q2) Product 6. https://landweb.modaps.eosdis.nasa.gov/QA_WWW/forPage/user_guide/MCD12Q2_Collection6_UserGuide.pdf.

Guan, K., Wood, E.F., Medvigy, D., Kimball, J., Pan, M., Caylor, K.K., Sheffield, J., Xu, X., Jones, M.O., 2014. Terrestrial hydrological controls on land surface phenology of African savannas and woodlands. J. Geophys. Res. Biogeosci. 119, 1–18. https://doi.org/10.1002/2013JG002572.Received.

Hall, D.K., Riggs, G.A., 1995. Mapping global snow cover using Moderate Resolution Imaging Spectroradiometer (MODIS) data. Remote Sens. Environ. 54, 127–140.

Hanes, J.M., Schwartz, M.D., 2011. Modeling land surface phenology in a mixed temperate forest using MODIS measurements of leaf area index and land surface temperature. Theor. Appl. Climatol. 105, 37–50. https://doi.org/10.1007/s00704-010-0374-8.

Hassan, Q.K., Rahman, K.M., 2013. Remote sensing-based determination of understory grass greening stage over boreal forest. J. Appl. Remote Sens. 7, 73578.

Helman, D., 2018. Land surface phenology: what do we really 'see' from space? Sci. Total Environ. https://doi.org/10.1016/j.scitotenv.2017.07.237.

Henebry, G.M., de Beurs, K.M., 2013. Remote sensing of land surface phenology: a prospectus. In: Schwartz, M. (Ed.), Phenology: An Integrative Environmental Science. Springer, Dordrecht. https://doi.org/10.1007/978-94-007-6925-0_21.

Hou, X., Gao, S., Sui, X., Liang, S., Wang, M., 2018. Changes in day and night temperatures and their asymmetric effects on vegetation phenology for the period of 2001-2016 in Northeast China. Can. J. Remote Sens. 44, 629–642. https://doi.org/10.1080/07038992.2019.1578204.

Huang, C., He, H.S., Liang, Y., Wu, Z.W., 2018. Effects of climate change, fire and harvest on carbon storage of boreal forests in the Great Xing'an Mountains, China. Chinese J. Appl. Ecol. 29, 2088–2100. https://doi.org/10.13287/j.1001-9332.201807.036.

Huete, A., Didan, K., Miura, T., Rodriguez, E.P., Gao, X., Ferreira, L.G., 2002. Overview of the radiometric and biophysical performance of the MODIS vegetation indices. Remote Sens. Environ. 83, 195–213. https://doi.org/10.1016/S0034-4257(02)00096-2.

Hwang, T., Song, C., Vose, J.M., Band, L.E., 2011. Topography-mediated controls on local vegetation phenology estimated from MODIS vegetation index. Landsc. Ecol. 26, 541–556. https://doi.org/10.1007/s10980-011-9580-8.

Janatian, N., Sadeghi, M., Sanaeinejad, S.H., Bakhshian, E., Farid, A., Hasheminia, S.M., Ghazanfari, S., 2017. A statistical framework for estimating air temperature using MODIS land surface temperature data. Int. J. Climatol. 37, 1181–1194. https://doi.org/10.1002/joc.4766.

Jeganathan, C., Dash, J., Atkinson, P.M., 2014. Remotely sensed trends in the phenology of northern high latitude terrestrial vegetation, controlling for land cover change and vegetation type. Remote Sens. Environ. 143, 154–170. https://doi.org/10.1016/j.rse.2013.11.020.

Jeong, S.J., Ho, C.H., Gim, H.J., Brown, M.E., 2011. Phenology shifts at start vs. end of growing season in temperate vegetation over the Northern Hemisphere for the period 1982-2008. Glob. Chang. Biol. 17, 2385–2399. https://doi.org/10.1111/j.1365-2486.2011.02397.x.

Jia, K., Liang, S., Wei, X., Li, Q., Du, X., Jiang, B., Yao, Y., Zhao, X., Li, Y., 2015. Fractional forest cover changes in Northeast China from 1982 to 2011 and its relationship with climatic variations. IEEE J. Sel. Top. Appl. Earth Obs. Remote Sens. 8, 775–783. https://doi.org/10.1109/JSTARS.2014.2349007.

Jönsson, P., Eklundh, L., 2004. TIMESAT - A program for analyzing time-series of satellite sensor data. Comput. Geosci. 30, 833–845. https://doi.org/10.1016/j.cageo.2004.05.006.

Jönsson, P., Eklundh, L., 2002. Seasonality extraction by function fitting to time-series of satellite sensor data. IEEE Trans. Geosci. Remote Sens. 40, 1824–1832. https://doi.org/10.1109/TGRS.2002.802519.

Liang, L., Henebry, G.M., Liu, L., Zhang, X., Hsu, L., 2021. Trends in land surface phenology across the conterminous United States (1982-2016) analyzed by NEON domains. Ecol. Appl. 0, 1–19. https://doi.org/10.1002/eap.2323.

Liu, J., Li, S., Ouyang, Z., Tam, C., Chen, X., 2008. Ecological and socioeconomic effects of China's policies for ecosystem services. Proc. Natl. Acad. Sci. U. S. A. 105, 9477–9482. https://doi.org/10.1073/pnas.0706436105.

Liu, Q., Fu, Y.H., Zhu, Z., Liu, Y., Liu, Z., Huang, M., Janssens, I.A., Piao, S., 2016. Delayed autumn phenology in the Northern Hemisphere is related to change in both climate and spring phenology. Glob. Chang. Biol. 22, 3702–3711. https://doi.org/10.1111/gcb.13311.

Lv, S.H., Ye, S.X., Zheng, Z.R., Liu, J.D., Feng, C.Y., 2012. The Forest-Steppe Ecotone in Northern China. China Environmental Science Press, Beijing.

Ma, J., Bu, R., Liu, M., Chang, Y., Han, F., Qin, Q., Hu, Y., 2016. Recovery of understory vegetation biomass and biodiversity in burned larch boreal forests in Northeastern China. Scand. J. For. Res. 31, 382–393. https://doi.org/10.1080/02827581.2015.1072238.

Ma, X., Huete, A., Yu, Q., Coupe, N.R., Davies, K., Broich, M., Ratana, P., Beringer, J., Hutley, L.B., Cleverly, J., Boulain, N., Eamus, D., 2013. Spatial patterns and temporal dynamics in savanna vegetation phenology across the North Australian Tropical Transect. Remote Sens. Environ. 139, 97–115. https://doi.org/10.1016/j.rse.2013.07.030.

Mackenzie, L.L., Bao, K., Pratte, S., Klamt, A.M., Liu, R., Aquino-López, M.A., Zawadzki, A., Amiri, B.J., Shen, J., Le Roux, G., 2021. Environmental change and human land-use over the past 200 years in the Great Hinggan Mountains. Northeastern China. L. Degrad. Dev. 32, 993–1007. https://doi.org/10.1002/ldr.3749.

Mann, H.B., 1945. Nonparametric tests against trend. Econometrica 13, 245–259. https://doi.org/10.2307/1907187.

Menzel, A., Sparks, T.H., Estrella, N., Koch, E., Aaasa, A., Ahas, R., Alm-Kübler, K., Bissolli, P., Braslavská, O., Briede, A., Chmielewski, F.M., Crepinsek, Z., Curnel, Y., Dahl, Å., Defila, C., Donnelly, A., Filella, Y., Jatczak, K., Måge, F., Mestre, A., Nordli, Ø., Peñuelas, J., Pirinen, P., Remišová, V., Scheifinger, H., Striz, M., Susnik, A., Van Vliet, A.J.H., Wielgolaski, F.E., Zach, S., Zust, A., 2006. European phenological response to climate change matches the warming pattern. Glob. Chang. Biol. 12, 1969–1976. https://doi.org/10.1111/j.1365-2486.2006.01193.x.

Misra, G., Buras, A., Heurich, M., Asam, S., Menzel, A., 2018. LiDAR derived topography and forest stand characteristics largely explain the spatial variability observed in MODIS land surface phenology. Remote Sens. Environ. 218, 231–244. https://doi.org/10.1016/j.rse.2018.09.027.

Peng, D., Wang, Y., Xian, G., Huete, A.R., Huang, W., Shen, M., Wang, F., Yu, L., Liu, L.Y., Xie, Q., Liu, L.L., Zhang, X., 2021. Investigation of land surface phenology detections in shrublands using multiple scale satellite data. Remote Sens. Environ. 252 https://doi.org/10.1016/j.rse.2020.112133.

Peng, D., Zhang, X.Y., Zhang, B., Liu, L., Liu, X., Huete, A.R., Huang, W., Wang, S., Luo, S., Zhang, X., Zhang, H., 2017. Scaling effects on spring phenology detections

from MODIS data at multiple spatial resolutions over the contiguous United States. ISPRS J. Photogramm. Remote Sens. 132, 185–198. https://doi.org/10.1016/j.isprsjprs.2017.09.002.

Piao, S., Fang, J., Zhou, L., Ciais, P., Zhu, B., 2006. Variations in satellite-derived phenology in China's temperate vegetation. Glob. Chang. Biol. 12, 672–685. https://doi.org/10.1111/j.1365-2486.2006.01123.x.

Piao, S., Liu, Q., Chen, A., Janssens, I.A., Fu, Y., Dai, J., Liu, L., Lian, X., Shen, M., Zhu, X., 2019. Plant phenology and global climate change: current progresses and challenges. Glob. Chang. Biol. https://doi.org/10.1111/gcb.14619.

Pisek, J., Rautiainen, M., Nikopensius, M., Raabe, K., 2015. Estimation of seasonal dynamics of understory NDVI in northern forests using MODIS BRDF data: semi-empirical versus physically-based approach. Remote Sens. Environ. 163, 42–47. https://doi.org/10.1016/j.rse.2015.03.003.

Reed, B.C., Schwartz, M.D., Xiao, X., 2009. Remote sensing phenology. In: Noormets A. (eds) Phenology of Ecosystem Processes. Springer, New York, NY. https://doi.org/10.1007/978-1-4419-0026-5_10.

Ren, S., Yi, S., Peichl, M., Wang, X., 2018. Diverse responses of vegetation phenology to climate change in different Grasslands in Inner Mongolia during 2000-2016. Remote Sens. 10 https://doi.org/10.3390/rs10010017.

Richardson, A.D., O'Keefe, J., 2009. Phenological Differences Between Understory and Overstory. In: Noormets, A. (Ed.), Phenology of Ecosystem Processes. Springer, New York, NY. https://doi.org/10.1007/978-1-4419-0026-5_4.

Sen, P.K., 1968. Estimates of the Regression Coefficient Based on Kendall's Tau. J. Am. Stat. Assoc. 63, 1379–1389. https://doi.org/10.1080/01621459.1968.10480934.

Shabanov, N.V., Zhou, L., Knyazikhin, Y., Myneni, R.B., Tucker, C.J., 2002. Analysis of interannual changes in northern vegetation activity observed in AVHRR data from 1981 to 1994. IEEE Trans. Geosci. Remote Sens. 40, 115–130. https://doi.org/10.1109/36.981354.

Song, X.P., Huang, C., Sexton, J.O., Channan, S., Townshend, J.R., 2014. Annual detection of forest cover loss using time series satellite measurements of percent tree cover. Remote Sens. 6, 8878–8903. https://doi.org/10.3390/rs6098878.

Tang, H., Li, Z., Zhu, Z., Chen, B., Zhang, B., Xin, X., 2015. Variability and climate change trend in vegetation phenology of recent decades in the Greater Khingan Mountain area. Northeastern China. Remote Sens. 7, 11914–11932. https://doi.org/10.3390/rs70911914.

Theil H. 1992. A Rank-Invariant Method of Linear and Polynomial Regression Analysis. In: Raj B., Koerts J. (eds) Henri Theil's Contributions to Economics and Econometrics. Advanced Studies in Theoretical and Applied Econometrics, Vol 23. Springer, Dordrecht. https://doi.org/10.1007/978-94-011-2546-8_20.

Tomaszewska, M.A., Henebry, G.M., 2020. How much variation in land surface phenology can climate oscillation modes explain at the scale of mountain pastures in Kyrgyzstan? Int. J. Appl. Earth Obs. Geoinf. 87, 102053 https://doi.org/10.1016/j.jag.2020.102053.

Tomaszewska, M.A., Nguyen, L.H., Henebry, G.M., 2020. Land surface phenology in the highland pastures of montane Central Asia: interactions with snow cover seasonality and terrain characteristics. Remote Sens. Environ. 240, 111675 https://doi.org/10.1016/j.rse.2020.111675.

Tong, X., Tian, F., Brandt, M., Liu, Y., Zhang, W., Fensholt, R., 2019. Trends of land surface phenology derived from passive microwave and optical remote sensing systems and associated drivers across the dry tropics 1992-2012. Remote Sens. Environ. 232, 111307 https://doi.org/10.1016/j.rse.2019.111307.

Townshend, J., Hansen, M., Carroll, M., DiMiceli, C., Sohlberg, R., Huang, C., 2015. User Guide for the MODIS Vegetation Continuous Fields product Collection 6, version 1. https://lpdaac.usgs.gov/documents/112/MOD44B_User_Guide_V6.pdf?_ga=2.233465051.452363763.1610418140-1369816519.1601179348.

Tremblay, N.O., Larocque, G.R., 2001. Seasonal dynamics of understory vegetation in four eastern Canadian forest types. Int. J. Plant Sci. 162, 271–286.

Tucker, C.J., Slayback, D.A., Pinzon, J.E., Los, S.O., Myneni, R.B., Taylor, M.G., 2001. Higher northern latitude normalized difference vegetation index and growing season trends from 1982 to 1999. Int. J. Biometeorol. 45, 184–190. https://doi.org/10.1007/s00484-001-0109-8.

Wan, Z., Hook, S., Hulley, G., 2015. MOD11A2 MODIS/Terra Land Surface Temperature/Emissivity 8-Day L3 Global 1km SIN Grid V006 [Data set]. NASA EOSDIS Land Processes DAAC. https://doi.org/10.5067/MODIS/MOD11A2.006.

Wang, J., Zhang, X., Rodman, K., 2021. Land cover composition, climate, and topography drive land surface phenology in a recently burned landscape: an application of machine learning in phenological modeling. Agric. For. Meteorol. 108432, 304–305. https://doi.org/10.1016/j.agrformet.2021.108432.

Wang, X.Y., Zhao, C.Y., Jia, Q.Y., 2013. Impacts of climate change on forest ecosystems in Northeast China. Adv. Clim. Chang. Res. 4, 230–241. https://doi.org/10.3724/SP.J.1248.2013.230.

White, M.A., de Beurs, K.M., Didan, K., Inouye, D.W., Richardson, A.D., Jensen, O.P., O'Keefe, J., Zhang, G., Nemani, R.R., van Leeuwen, W.J.D., Brown, J.F., de Wit, A., Schaepman, M., Lin, X., Dettinger, M., Bailey, A.S., Kimball, J., Schwartz, M.D., Baldocchi, D.D., Lee, J.T., Lauenroth, W.K., 2009. Intercomparison, interpretation, and assessment of spring phenology in North America estimated from remote sensing for 1982-2006. Glob. Chang. Biol. 15, 2335–2359. https://doi.org/10.1111/j.1365-2486.2009.01910.x.

White, M.A., Hoffman, F., Hargrove, W.W., Nemani, R.R., 2005. A global framework for monitoring phenological responses to climate change. Geophys. Res. Lett. 32, 1–4. https://doi.org/10.1029/2004GL021961.

Wu, R., Zhang, H., Zhao, J., Shan, Y., Guo, X., Ying, H., Deng, G., Li, H., 2021. Promote the advance of the start of the growing season from combined effects of climate change and wildfire. Ecol. Indic. 125, 107483 https://doi.org/10.1016/j.ecolind.2021.107483.

Yang, Y.Z., Cai, W.H., Yang, J., 2017. Evaluation of MODIS land surface temperature data to estimate near-surface air temperature in Northeast China. Remote Sens. 9, 410. https://doi.org/10.3390/rs9050410.

Yu, L., Zhang, S., Liu, T., Tang, J., Bu, K., Yang, J., 2015. Spatio-temporal pattern and spatial heterogeneity of ecotones based on land use types of southeastern Da Hinggan Mountains in China. Chinese Geogr. Sci. 25, 184–197. https://doi.org/10.1007/s11769-014-0671-8.

Zhang, G., Xiao, X., Dong, J., Kou, W., Jin, C., Qin, Y., Zhou, Y., Wang, J., Menarguez, M. A., Biradar, C., 2015. Mapping paddy rice planting areas through time series analysis of MODIS land surface temperature and vegetation index data. ISPRS J. Photogramm. Remote Sens. 106, 157–171. https://doi.org/10.1016/j.isprsjprs.2015.05.011.

Zhang, X., Friedl, M.A., Schaaf, C.B., Strahler, A.H., 2004. Climate controls on vegetation phenological patterns in northern mid- and high latitudes inferred from MODIS data. Glob. Chang. Biol. 10, 1133–1145. https://doi.org/10.1111/j.1529-8817.2003.00784.x.

Zhang, X., Liu, L., Henebry, G.M., 2019. Impacts of land cover and land use change on long-term trend of land surface phenology: a case study in agricultural ecosystems. Environ. Res. Lett. 14 https://doi.org/10.1088/1748-9326/ab04d2.

Zhang, X., Wang, J., Gao, F., Liu, Y., Schaaf, C., Friedl, M., Yu, Y., Jayavelu, S., Gray, J., Liu, L., 2017. Exploration of scaling effects on coarse resolution land surface phenology. Remote Sens. Environ. 190, 318–330.

Zhu, W., Lű, A., Jia, S., Yan, J., Mahmood, R., 2017. Retrievals of all-weather daytime air temperature from MODIS products. Remote Sens. Environ. 189, 152–163. https://doi.org/10.1016/j.rse.2016.11.011.

Vermote, E., 2015. MOD09A1 MODIS/Terra Surface Reflectance 8-Day L3 Global 500m SIN Grid V006 [Data set]. NASA EOSDIS Land Processes DAAC. https://doi.org/10.5067/MODIS/MOD09A1.006.